JOURNAL OF MATERIALS SCIENCE 14 (1979) 705–711

Reaction hot-pressing of zircon–alumina mixtures

E. DI RUPO
Department of Materials Science, University of Mons, 15 Av. Maistriau, 7000 Mons, Belgium

E. GILBART, T. G. CARRUTHERS, R. J. BROOK
Department of Ceramics, University of Leeds, Leeds, UK

Measurements have been made of the concurrent rates of reaction and of densification during the hot-pressing of mixtures of alumina and zircon powders. The results can be interpreted in terms of a liquid-phase sintering model and evidence is presented for separable stages of particle rearrangement, diffusion-controlled densification and residual reaction subsequent to attainment of zero porosity.

1. Introduction

The zircon–alumina system is of interest for many high temperature applications, especially in the glass industry [1, 2]. Materials based on this system are usually prepared either by fusion casting [3] or by pressureless reaction sintering [4, 5]. Miyatake, *et al.* [6] and Kobayashi and Oyama [7] have proposed a mechanism for the reaction occurring during firing. No mechanism for densification or for combined densification and reaction has yet been proposed.

Usually, the co-existence of alternative mechanisms for pressureless sintering or for hot-pressing [8–10] complicates the interpretation of sintering kinetics. Moreover, when a chemical reaction occurs *in situ* the progress of the reaction can additionally modify the process of densification [11]. However, when both reaction and densification involve diffusion of the same species, measurements of the kinetics of reaction and of densification may provide complementary information concerning the diffusion process, so that the presence of the reaction may serve to clarify the process responsible for densification. This approach has been adopted in treating the simultaneous α/β phase transition and densification during the hot-pressing of silicon nitride [12]; in that instance, however, the reaction need not *a priori* involve a diffusion step and it is consequently of interest to study a true chemical reaction, in which mass transfer must necessarily occur, in order to explore the approach less ambiguously.

In the present work, an attempt is made to exploit the information provided by the co-existence of a chemical reaction and sintering in seeking a picture of the controlling atomic mechanisms in the processing of zircon/alumina ceramics.

2. Experimental details

2.1. Materials

The raw materials used were Australian zircon of more than 99 wt% purity, obtained from S.C.R. Sibelco-Antwerpen, Belgium, and tabular alumina of more than 99.5 wt% purity, obtained from Alcoa, Int, the Netherlands; the zircon was further purified by treatment with methyl alcohol and with sulphuric acid.

Spectrographic analysis showed the following levels of impurity: Al_2O_3 0.4 wt%, TiO_2 0.1 wt%, FeO 0.1 wt%, CaO 0.04 wt%, MgO 0.04 wt%, Na_2O 0.02 wt%, and K_2O 0.02 wt% in the zircon, and CaO 0.06 wt%, MgO 0.06 wt%, Na_2O 0.08 wt%, and K_2O 0.08 wt% in the alumina.

The initial size distributions of the zircon and alumina powders were measured with a laser granulometer (Compagnie Industrielle de Lasers, Type 226). The grain size varied from 0.1 to 10 μm for the zircon and from 0.1 to 15 μm for the alumina, the average grain sizes being 3 and

1 μm respectively. Scanning electron micrographs of the particles confirmed the sizes measured but revealed aggregates of equi-axed grains in both cases.

The powders were mixed with methyl alcohol for 12 h, dried and hot-pressed at 1450° C under different pressures. For the observation of the influence of a flux, dried Na_2CO_3 was added to a mixture of the powders in alcohol, the ternary mixture being then dried and calcined at 1000° C for 5 h before hot-pressing.

2.2. Hot-pressing

The details of the hot-pressing apparatus and its associated equipment have been published previously [13]. About 14 g mixed powders were placed in a nuclear grade graphite die with all internal surfaces protected by a layer of high purity boron nitride. The intended hot-pressing pressure was applied to the cold compact and released. The die was then heated to 1450° C in about 13 min. When the hot-pressing temperature was reached, the pressure was reapplied and a stable value was reached within about 3 sec.

The progress of densification was measured from the movement of the hydraulic pressing ram using a linear variable displacement transducer connected to an ultraviolet recording galvanometer, so that very rapid density changes could be followed. The temperature was maintained to within ± 5° C, and the pressures were held to within ± 1 MN m^{-2} using a gas ballasted hydraulic accumulator. At the end of the hot-pressing cycle, cooling was sufficiently rapid to prevent any significant advance of the reaction between the alumina and zircon.

2.3. X-ray analysis

X-ray diffraction measurement was performed with a Philips PW 1130 X-ray diffractometer. The hot-pressed samples were ground and screened to produce powders with a particle size below 30 μm. Quantitative analysis of the various phases present after hot-pressing was carried out by comparing the relative intensities of the strongest diffraction lines of, respectively, tetragonal zircon (1 1 3), monoclinic zirconia (1 1 1), orthorhombic mullite (2 1 0) and hexagonal alumina (1 1 3). NaF (2 0 0) was used as an internal standard, the calibration curves being obtained from X-ray diffraction patterns of mixtures of zircon, alumina, zirconia, mullite and NaF of known composition. A tentative estimation of the accuracy of the quantitative analysis indicated that compositions could be determined to within ± 3 wt %.

2.4. Density measurements

The bulk density of every hot-pressed sample was measured by both mercury and water displacement. True densities were calculated using the phase composition as given by X-ray diffraction together with the true density values of zircon, alumina, zirconia and mullite, namely 4630, 3850, 5680 and 3160 kg m^{-3}, respectively. In order to check the values of these calculated true densities, a complete set of direct density measurements was performed on crushed samples using a pycnometer. The observed experimental densities were found to be in good agreement with the calculated values.

3. Results and discussion

The reaction between zircon and alumina follows the equation

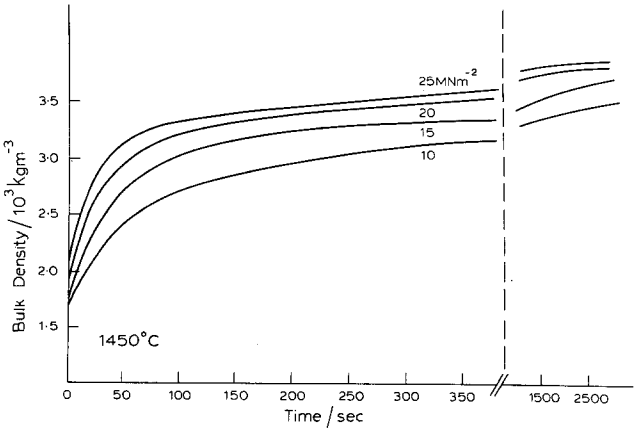

Figure 1 Time-dependence of apparent density for zircon–alumina at 1450° C under pressures of 10, 15, 20 and 25 MN m^{-2}.

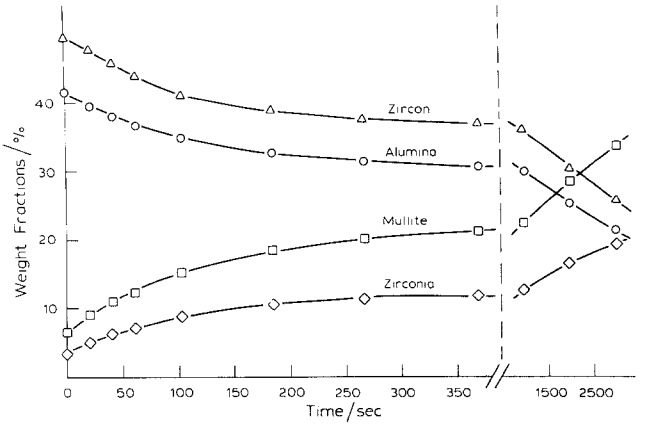

Figure 2 Variation of the amounts of products and reactants with time at 1450° C under a pressure of 15 MN m^{-2}.

$$2ZrSiO_4 + 3Al_2O_3 \rightarrow 2ZrO_2 + 2SiO_2 \cdot 3Al_2O_3. \quad (1)$$

Molar quantities of zircon and alumina corresponding to this stoichiometric reaction were used in the preparation of all samples. The latter were then hot-pressed at 1450° C under different pressures for various times.

Fig. 1 illustrates the variation of the bulk density, ρ_b, with time for zircon–alumina samples hot-pressed at 1450° C under pressures of 10, 15, 20 and 25 MN m^{-2}. Each curve shows a rapid initial densification rate which decreases continuously. At the temperature used, the rates of densification are seen to be markedly pressure-dependent.

Under comparable conditions, the progress of the reaction between zircon and alumina can also be traced. For instance, Fig. 2 shows the variation of the amounts (wt%) of zircon, alumina, zirconia and mullite, as measured by X-ray analysis, for specimens hot-pressed at 1450° C under a pressure of 15 MN m^{-2}. By the time the pressure has reached its steady value, it can be seen that some reaction has already taken place.

Since the ratio

$$\left(\frac{m \cdot w}{\rho_{th}}\right)_{ZrSiO_4} : \left(\frac{m \cdot w}{\rho_{th}}\right)_{Al_2O_3} = 0.67 = 2:3$$

where $m \cdot w$ is the molecular weight and ρ_{th} the true density, it can be seen from the reaction equation that equal volumes of alumina and of zircon are consumed in the stoichiometric reaction. Fig. 3 displays the decrease of volume of alumina with time. Like the rates of densification, the rates of reaction are pressure-dependent.

As a consequence of the simultaneous occurrence of the chemical reaction, the true density, ρ_{th}, i.e. the value that would correspond to a fully dense sample, changes continuously with time during hot-pressing. The scale of this change can be indicated by the values for the initial composition and for the fully reacted condition which are 4250 and 3760 kg m^{-3}, respectively. Accordingly, to estimate the change in the relative density, $\rho = \rho_b/\rho_{th}$ with time, the observed bulk densities in Fig. 1 must be related to the instantaneous values of ρ_{th} which can be calculated from the phase composition as given in Fig. 2.

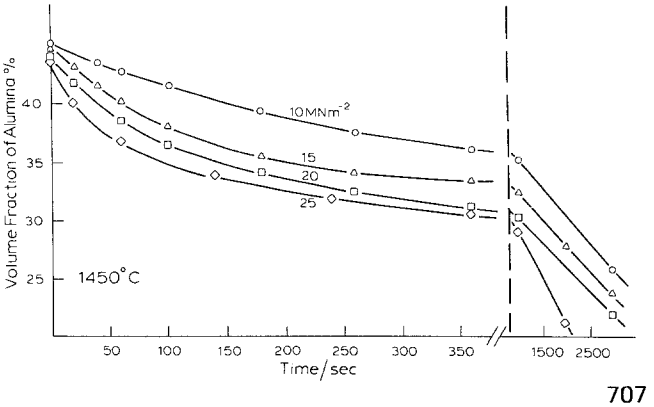

Figure 3 Quantity of alumina consumed during the hot-pressing of zircon–alumina mixtures.

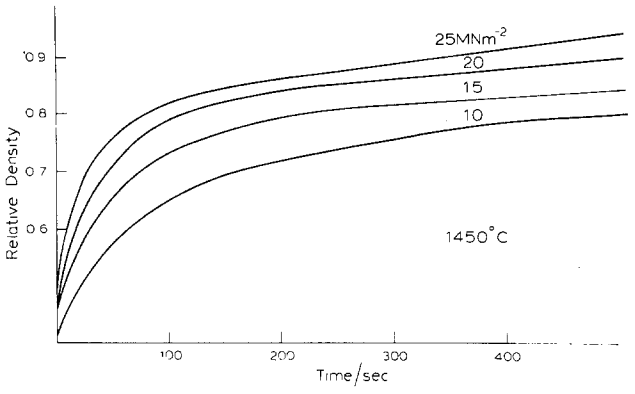

Figure 4 Densification data for zircon–alumina at 1450° C under pressures of 10, 15, 20, 25 MN m^{-2}.

Figure 4 shows the variation of these relative densities with time for different applied pressures. The densification results can be interpreted in terms of a model for boundary-phase assisted hot-pressing [14] based on Coble's creep equation [15, 16]

$$\frac{d\rho}{dt} = \frac{47.5 D_b w \Omega}{L^3 kT} P_A \qquad (2)$$

where D_b is the controlling diffusion coefficient in the boundary phase, w is the width of the boundary phase, L is the grain size, Ω the volume of zircon and alumina transported by one atom of the rate-controlling species, and P_A the applied pressure.

Under conditions of constant grain size and constant boundary thickness (impurity content), the densification rate calculated at a particular value of the relative density should, according to the model, show a linear dependence on the applied pressure. Data taken at $\rho = 0.75$ are shown in Fig. 5, and it can be seen that agreement with a linear dependence is reasonable although a small positive intercept on the pressure axis is indicated. In respect to this last feature, it may be noted that under conditions of pressureless treatment, the zircon–alumina reaction has been observed [17] to give rise to an expansion in samples of comparable density.

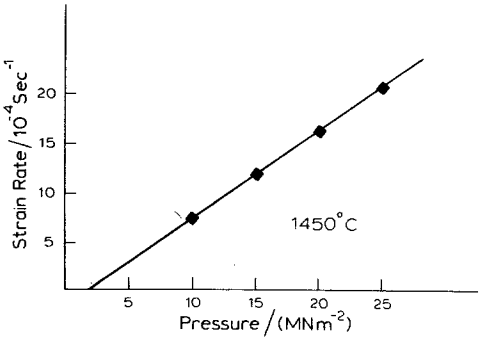

Figure 5 Pressure-dependence of the instantaneous densification rate derived from Fig. 4 at a relative density of 0.75.

In order to study the influence of the boundary thickness, w, a flux (Na_2O) was added to increase the quantity of boundary phase. Analysis of the densification curves obtained at 1450° C under an applied pressure of 20 MN m^{-2} at varying Na_2O levels, shown in Fig. 6, demonstrates that the increase in densification rate is linearly dependent on the quantity of Na_2O added (Fig. 7). The most direct explanation of this dependence is that w in Equation 2 is given by

$$w = w_0 + k(c_{Na_2O}) \qquad (3)$$

where w_0 is the boundary thickness in the undoped sample and c_{Na_2O} is the concentration of Na_2O (wt%) added. The indication from the figure is that w_0 is comparable in extent to the width contributed by an addition of some 0.25% Na_2O; reference to the levels of impurity in the starting materials (0.22% $MO + M_2O$ in the zircon and 0.28% in the alumina) gives support to this view. The ostensibly undoped materials already contain fluxing oxides in magnitudes comparable to the levels of additive employed.

The above results (Figs. 5 and 7) suggest that for the processing stage corresponding to the chosen densities ($\rho \sim 0.75$), the densification data can be interpreted in terms of the proposed model. This, in turn, suggests that the atomic mechanism for densification under these conditions is one of solution of the reacting species in a boundary phase, diffusion in the boundary phase from the intergrain region away to the region surrounding a pore, and reprecipitation from the boundary phase to give the product phases. A schematic diagram of the reaction geometry is given in Fig. 8. In line with the dependence shown in Fig. 5,

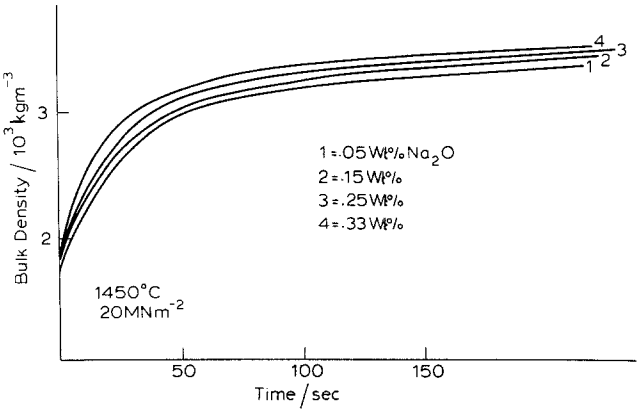

Figure 6 Densification curves for zircon–alumina with varying Na_2O content.

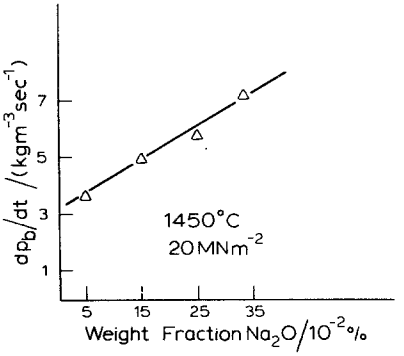

Figure 7 Dependence of instantaneous densification rate of zircon–alumina on the variation of Na_2O content.

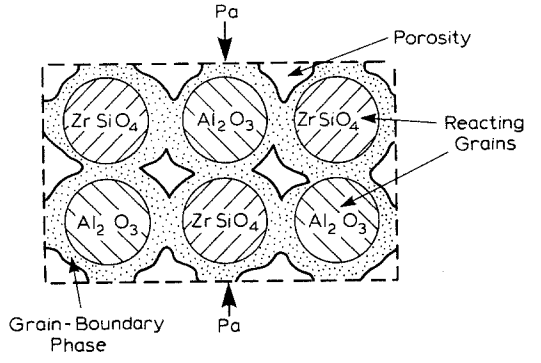

Figure 8 A view of the microstructure associated with the proposed model. The reacting grains are spheres, and material diffuses from the intergrain regions, through the boundary phase, to the grain surfaces adjacent to the pores.

diffusion appears to be the rate limiting step in the reaction sequence.

Using Equation 2, an approximate figure for the controlling diffusion coefficient can be estimated. If it is assumed that the added Na_2O forms a boundary phase of composition $Na_2O{\cdot}2SiO_2$ and that it is uniformly distributed at the boundary, then $w \approx 8 \times 10^{-9}$ m for grain size, L, $\approx 2 \times 10^{-6}$ m and for an additive content of 0.25% by weight Na_2O. With $k = 1.38 \times 10^{-23}$ J K^{-1}, $T = 1723$ K, $P_a = 2 \times 10^7$ N m^{-2}, and $\Omega \approx 1.32 \times 10^{-28}$ (assuming control by Si^{4+} diffusion; slight variations occur for control by Zr^{4+}, O^{2-}, or Al^{3+}), use of the densification rate of 1.5×10^{-3} sec^{-1} (Fig. 7) suggests a figure for the diffusion coefficient of $\sim 3 \times 10^{-13}$ m^2 sec^{-1}. This figure is somewhat lower than expected for a vitreous boundary phase; the discrepancy can perhaps best be accounted for in terms of non-uniformities in the distribution of the second phase at the boundaries.

The range of densities over which the proposed model applies can be estimated by comparing the rate of reaction and the rate of densification at different stages during processing. For the solution–diffusion–reprecipitation sequence, these rates are linked [18] by the relationship:

$$\frac{1}{\rho_t}\frac{d\rho}{dt} = -\frac{G}{S}\frac{1}{V_t}\frac{dV}{dt} \qquad (4)$$

where ρ and V represent the density of the compact and the volume concentration of one of the original constituent phases, respectively. S is the propability that a diffusing atom partaking in the densification process is also involved in the chemical reaction, and G is a factor which depends on the specific geometry. In the Coble model for deformation by grain-boundary diffusion, G has the value 2/3. The subscript t represents use of the instantaneous values of ρ and V at the time, t. The equation is based on the argument that, since a reaction occurs simultaneously with densification, the volume of material moved can be represented both in terms of the volume of material engaged in the reaction and in terms of the volume flux giving rise to densification.

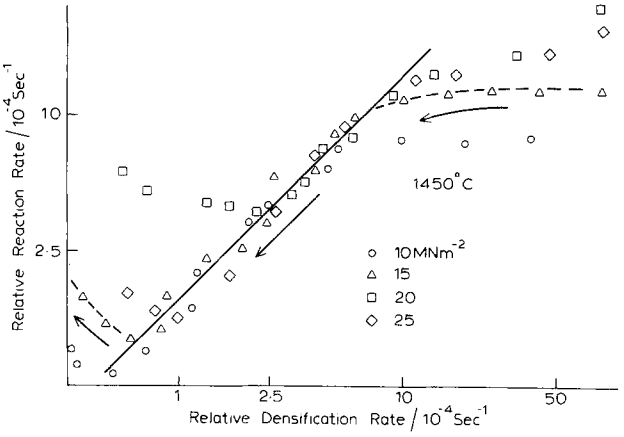

Figure 9 Relationship between densification rate and reaction rate for samples prepared at different pressures; each point represents data taken at a particular time, and the arrows indicate the direction of increasing time.

To test the validity of the equation, the simultaneous rates of densification and reaction are obtained from Figs. 1 and 3 at different times and plotted together as in Fig. 9. Where both processes occur by the solution–diffusion–reprecipitation path, the plotted points should, from Equation 4, fall on the solid line which has a slope of unity and which intercepts the unit densification rate line at a transformation rate of 1.5. Observation of such a dependence would indicate first the dominance of the proposed densification mechanism over possible alternatives and secondly the fact that each diffusing atom takes part in both densification and the chemical reaction.

From Fig. 9 three stages in the overall process can be distinguished similar to those proposed for the liquid-phase sintering cycle [19] of a non-reacting system. In the first part, the relative rate of densification is higher than the value predicted by the observed relative rate of reaction using Equation 4. This indicates that the degree of densification is greater than can be caused by atom diffusion processes alone. The most probable mechanism is that of particle rearrangement such as can proceed by viscous sliding between particles bonded together by a liquid phase. In this connection, it is known that the influence of a liquid phase on the rearrangement of grains may be detected even in the presence of a small volume fraction of liquid phase (less than 0.01 mol %) [20]. Such a volume fraction of liquid is not inconsistent with the amount expected in the zircon–alumina system where the stated quantities of impurity are present [21, 22].

In the second stage, between relative densities of 0.7 and 0.9 approximately, the two relative rates are in close agreement with the ratio expected on the basis of the diffusion-limited densification model. This is the stage represented earlier in Figs. 5 and 7 in which the atom, diffusing down the stress gradient created by the applied pressure, is seen at the same time as contributing to the chemical reaction.

In the third stage, the relative rate of densification decreases while the reaction continues. The reactive atoms are no longer entirely associated with densification, a situation attributable to the continued reacting of grain cores in completely densified regions of the sample.

Fig. 10 shows a diagram constructed for 1450° C from Fig. 9 which maps the pressure and density dependence of the three stages corresponding to the distinguishable rate-controlling mechanisms which occur in the hot-pressing of zircon–alumina powders. The analogy between

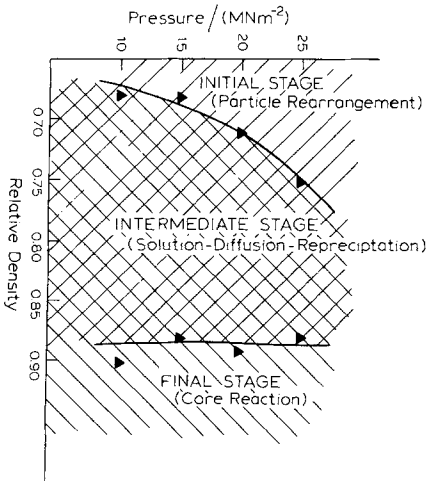

Figure 10 Diagram showing the three zones of reactive hot-pressing of zircon–alumina for 1450° C. The dominant mechanism is indicated for different conditions of applied pressure and sample density.

such a map and proposed hot-pressing maps [23] and deformation maps [24] will be apparent. Notable features are the appearance of particle rearrangement as one of the major mechanisms and the increased importance of this mechanism as the pressure is raised; this last trend is perhaps unexpected in view of the fact that particle rearrangement is usually considered to have a similar pressure-dependence [19] to the rival diffusional process. Models for particle rearrangement are, however, relatively undeveloped and it may be that non-viscous mechanisms can be significant.

4. Conclusions

In specific reference to the zircon–alumina mixtures concerned, the data suggest that densification is achieved first by particle rearrangement to an extent which is pressure-dependent but which ends at a relative density between 0.65 and 0.75, and secondly by particle reshaping achieved by solution, diffusion and reprecipitation of the constituent atoms in a high diffusivity boundary phase. The chemical reaction is achieved in both stages by dissolution of the reactants in the boundary phase followed by precipitation of the products.

More generally, the data demonstrate that, under conditions where a chemical reaction occurs by a process similar to one of the processes responsible for densification, a comparison of the rates of reaction and densification can be used to isolate the contribution made to densification by that process and hence to distinguish it from the contributions made by alternative mechanisms. Since the co-existence of alternative mechanisms is one of the major impediments to the successful quantitative analysis of densification data, this ability to distinguish the various contributions of the different mechanisms is of considerable potential value.

The limitations of the method lie in the restriction of its use to a particular range of systems. Thus it requires compositions in which a chemical reaction or a phase change is co-existent with densification. Further it requires that the reaction product be removed from the zone between the reacting particles so that the direct link between the rates of reaction and densification for the solution–diffusion–reprecipitation mechanism can apply; in this respect, it is expected that the method will be most appropriate for hot-pressing studies where the driving force for the removal of material from between the particles is relatively high.

Acknowledgement

We wish to thank F.N.R.S. (Belgium) and the British Council for a grant to one of us (E. Di Rupo).

References

1. E. R. BEGLEY and P. O. HERNDON, in "High Temperature Oxides" 5-IV, edited by A. M. Alper (Academic Press, New York, 1972) p. 185.
2. K. SHAW, "Refractories and their Uses" (Applied Science London, 1972) p. 238.
3. G. S. FULCHER, U.S. Patent No. 1 615 751 (1926).
4. E. A. THOMAS, U.S. Patent No. 90 229 (1961).
5. E. Di RUPO, M. R. ANSEAU, J. P. BILOQUE and P. FIERENS, Belgian Patent No. 181 362 (1977).
6. K. MIYATAKE, K. SEMBA and M. SEKIME, *Taikabutra* **21** (1969) 105.
7. A. KOBAYASHI and T. OYAMA, *ibid* **29** (1971) 59.
8. D. L. JOHNSON, *Mat. Sci. Res.* **6** (1973) 363.
9. R. M. SPRIGGS and S. K. DUTTA, *ibid* **6** (1973) 369.
10. R. J. BROOK, *Science of Ceramics* **9** (1978) 57.
11. R. PAMPUCH, "Ceramic Materials" (Elsevier, Amsterdam 1976) p. 151
12. L. J. BOWEN, R. J. WESTON, T. G. CARRUTHERS and R. J. BROOK, *J. Mater. Sci.* **13** (1978) 341.
13. R. J. WESTON and T. G. CARRUTHERS, *Proc. Brit. Ceram. Soc.* **22** (1973) 197.
14. L. J. BOWEN, R. J. WESTON, T. G. CARRUTHERS and R. J. BROOK, *Ceramurgia Int.* **2** (1976) 173.
15. R. L. COBLE, in "Sintering and Related Phenomena" edited by G. C. Kuczynski, (Gordon and Beach, New York, 1967) p. 329.
16 Idem, *J. Appl. Phys.* **34** (1963) 1679.
17. E. di RUPO, unpublished work.
18. L. J. BOWEN, T. G. CARRUTHERS and R. J. BROOK, *J. Amer. Ceram. Soc.* **61** (1978). 335.
19. W. D. KINGERY, *J. Appl. Phys.* **30** (1959) 301.
20. R. PAMPUCH, "Ceramic Materials" (Elsevier, Amsterdam 1976) p. 147.
21. E. M. LEVIN, C. E. ROBBINS and H. F. McMURDIE, "Phase Diagrams for Ceramics" (The American Ceramic Society, Columbus, 1964) pp. 156, 181, 241, 246.
22. E. M. LEVIN, C. E. ROBBINS and H. F. McMURDIE, *ibid* (1969) p. 64.
23. D. S. WILKINSON and M. F. ASHBY, *Mat. Sci. Res.* **10** (1975) 473.
24. T. G. LANGDON and F. A. MOHAMED, *J. Mater. Sci.* **11** (1976) 317.

Received 13 June and accepted 21 July 1978.